

DNS OF TRANSITIONAL BOUNDARY-LAYER FLOWS AT SUB- AND HYPERSONIC SPEEDS

Markus Kloker

Institut für Aerodynamik und Gasdynamik, Universität Stuttgart
Pfaffenwaldring 21, D-70550 Stuttgart

1. SUMMARY

In this paper recent highlight results of high-order direct numerical simulations (DNS) of controlled induced laminar-to-turbulent boundary-layer transition are presented. For a generic subsonic swept-back wing flow, subject to crossflow (CF) instability typically leading to early transition triggered by large-amplitude longitudinal (CF-)vortices, it is shown that transition can be successfully delayed by the technique of upstream flow deformation (UFD): Vortices with appropriately small spanwise spacing excited intentionally can suppress the naturally growing vortices and do not trigger the high-frequency secondary instability causing eventually transition. Indeed, the UFD technique challenges the currently favored method of suction. For the hypersonic flow over a flat-plate or cone it has been shown that wall-cooling by radiation, present at flight conditions but not at the typical "cold" wind tunnel conditions, favors a transition mechanism dominated by a large-amplitude, so-called acoustic (2-d) disturbance. Here it is shown that this high-frequency disturbance gives rise to local separation zones and shocklets inside the boundary layer close to the wall where the disturbances move faster than sound waves can travel. In the Mach 6.8 example discussed the wall temperature rises from 975K to 1200K, a peak value distinctly higher than the temperature at fully turbulent conditions.

2. INTRODUCTION

Direct numerical simulations (DNS) of high-order accuracy and resolution performed on super computers can enable undreamed-of insight in fundamental microscale or high-frequency flow phenomena. A paradigm is the simulation of the physically unstable, dynamical processes during laminar-turbulent transition in boundary-layer flows forming along aerodynamical bodies in flight. For fundamental studies generic laminar base flows on simple bodies like the flat plate, wedges, or cones are used, and transition is triggered by a well-defined disturbance input. This mimics so-called controlled experiments where the background disturbance level of the experimental facility is extremely low and special disturbance devices are used. Only results of such kind of experimental or numerical simulations enable lasting scientific progress. This also holds for (early-)turbulent flows. In this case the influence of unnoticed unsteady boundary conditions present in experiments or the basic numerical properties of the integration scheme used in the DNS or large-eddy simulation (LES) were and still are often underestimated. It is useless to tackle too complex a problem; rather the breakdown into smaller, more transparent units representing the physical basics is beneficial.

3. BASIC NUMERICAL ASPECTS OF DNS

Simple body geometries allow relatively simple numerical grids, and numerical resolution studies have to be truly convergent, i.e. the solution must tend to the correct one upon refining the grid if the method is numerically consistent. This has to be checked by comparisons with theories like the primary Linear Stability Theory, Secondary Stability Theories, or the Parabolized Stability Equations. In fact, such tests have to be done prior to the comparison with an experiment, because the method has first to be verified. Verification secures that the numerical method solves the underlying equations to some accuracy, whereas the validation process tests simultaneously and inseparably the chosen equations, including the fluid properties, boundary conditions, and some extra modeling, and their numerical solution. Typically, only DNS methods with an accuracy order of at least four can adequately cope with the problems at reasonable resolution. Low order methods, "compensated" by many (?) grid points will see severe trouble at advanced research stages. At the same accuracy order, compact or Padé methods are distinctly superior over standard methods in terms of resolution power, i.e. they need less grid points to accurately treat the fundamental wave(-like) solutions. This holds both for the viscous terms, connected to the second derivative, and the convection terms, connected to the first spatial derivative, if a finite difference (FD) scheme is used. It can even be useful not to employ all points of a stencil to maximize its accuracy order – the classical method – but to restrict it to 4th or 6th-order and use the remaining information to optimize its characteristics in Fourier space. For the convection part such schemes are sometimes called dispersion-relation preserving because also the Fourier modes with high grid-related wavenumbers $k^* = k\Delta x$, say greater than one, are correctly transported and the numerical dispersion is small. Think of a (smeared) Dirac pulse, that can be viewed as a full flat spectrum in Fourier space: A numerical method with good properties in the wave space will be able to transport this signal with much less error than standard methods. For compressible flow not too strong shocks can be equivalently handled; only in case of strong shocks an additional localized shock treatment by essentially non-oscillatory (ENO) schemes is appropriate.

Unlike linear problems, e.g. some acoustics, nonlinear problems benefit from a somewhat higher accuracy order rather than an optimization up to very large k^* . Here high wavenumber modes are often generated by and thus are slaves of low wavenumber modes, and the higher accuracy of the latter is useful. Moreover, a de-aliasing procedure is necessary because modes with $k^* > 2/3\pi$ generate, at quadratic nonlinearity, modes with $k^* > 4/3\pi$ that can spoil the modes with $k^* < 2/3\pi$ because the natural

limit for representation on the grid is the wiggle mode $k^*=\pi$, $\lambda=2\Delta x$. De-aliasing means removing relevant energy of these modes either by cutting off the spectrum by high-order compact filtering, or by some extra or inherent damping. The crucial point at this operation is that low wavenumber modes are to be unaltered, a property not intrinsic to classical extra damping (by a second-order FD of the fourth derivative) or upwind methods of an order lower than four.

The time integration scheme has to be A-stable for both types of derivatives. That means that explicit methods should be of at least 3rd order. Like for the spatial schemes the resolution properties for wave-like solutions are of crucial importance; the often cited A-stability limits do not directly correlate with this aspect. As for Runge-Kutta methods RKm-On, m steps, nth-order, RK4-O4 is clearly superior to RK3-O3 in terms of resolution power even with a time step 4/3 times the RK3-O3 step to compensate for the higher computational effort [1]. Inversely, the proper analysis of a reported "successfully" used scheme allows a conclusion of the properties of the underlying spatial discretization: If, for instance, a variant RK5-O2 is used that turns out to be optimized for a large diffusion-problem stability margin but has zero stability for a pure advection-type problem, the solved equations or their spatial discretization effectively represent an artificial, low Reynolds number problem. Equivalently important, the time integrator formulation should enable phase-accurate inclusion of unsteady boundary conditions. For some low-storage versions of Runge-Kutta methods this is not true because the time position of intermediate steps is undefined.

When implicit schemes are used recall that the possible stable solutions using large time steps can no more be accurate for some frequency components. Here, badly computed components have high spatial wave numbers for the viscous terms, but intermediate wave numbers only for the convection terms. (In the latter case the highest frequency arises from the numerically largest first spatial derivative which comes, depending on the spatial scheme used, from wave numbers smaller than $k^*=\pi$, see, e.g., [2].)

A subject of paramount importance is the outflow boundary treatment for spatially non-periodic problems. Even an advanced formulation based on characteristics theory in compressible flow, either in x-y or x-t space, does not allow, if applied alone, a reflection-free outflow. Some inclusion of buffer domains is necessary where the disturbances are artificially damped and/or where the equations are smoothly modified to simple hyperbolic behavior.

4. SUBSONIC 3-D BOUNDARY-LAYER FLOW: CF VORTICES AND THEIR CONTROL

On a swept-back airplane wing the chordwise acceleration of the upper-side flow induces an inboard-oriented crossflow component inside the boundary layer perpendicular to the meanflow direction. The combination of swept configuration and chordwise pressure gradient generates curved inviscid streamlines at the boundary-layer edge. Thus, a pressure gradient perpendicular to the streamlines exists. Inside the boundary layer the velocity goes to zero at the wall but the chordwise pressure

gradient keeps approximately constant. This imbalance results in a compensation-flow towards the inviscid streamline's centre of curvature, the so-called crossflow. The crossflow velocity profile $w(y)$, y being the wall-normal coordinate, is inflectional and causes a strong primary instability of the flow with respect to so-called crossflow (CF) modes, which can be steady or unsteady. The unsteady disturbances, CF-waves, have been found to be dominant at medium- to high-turbulence conditions, where they are excited on higher amplitude levels and can nonlinearly suppress the development of the unstable steady modes. At low freestream turbulence conditions as in free flight, steady crossflow vortex modes are found to be dominant, although the maximum primary amplification is for traveling disturbances. Obviously, the steady modes which are excited even by minute surface nonuniformity or roughness are significantly higher in amplitude right from start. Since this scenario is assumed to be the most relevant, most investigations concentrate on the steady-vortex dominated regime. Upon downstream amplitude saturation high-amplitude steady 'crossflow' vortices, being longitudinal vortices roughly aligned with the external streamline direction x_s , are formed which distort the flow field and trigger a subsequent 'explosive' secondary instability mechanism eventually leading to laminar breakdown.

The considered laminar base flow is designed to resemble the flow on the suction side of an infinite swept wing, with decreasing chordwise favorable pressure gradient and ensuing adverse pressure gradient. The streamwise edge velocity is defined analytically, also to facilitate the calculation of the boundary condition at the upper boundary of the integration domain on the flat plate. The sweep angle is $\varphi_{sw}=45^\circ$ and the crossflow component attains a maximum value of 13.3% of the edge velocity. For more details see [4].

4.1. Numerical method

The results are gained with a carefully tested 6th-order compact FD / spanwise Fourier-spectral scheme for spatial DNS in vorticity-velocity formulation of unsteady 3-d boundary-layer flows in a rectangular integration domain with periodic sidewise boundaries. First, the spanwise invariant steady base flow determined by the inflow profiles and a given chordwise edge velocity is calculated; next, defined disturbances are introduced in localized strips at the wall by blowing and suction, and their 3-d, asymmetric, (unsteady) development up to late stages of transition is simulated in a disturbance formulation. For time integration an RK4-O4 method is used.

The spanwise Fourier ansatz principally reduces the 3-d problem in physical space to a coupled set of (K+1) complex 2-d problems in Fourier space thus enabling a largely parallel computation in Fourier space. However the modes are coupled by the nonlinear convective terms of the vorticity transport equations and are transformed to physical space for the calculation of the nonlinear terms which in turn are parallelized in the streamwise direction. In this pseudospectral method for the nonlinear terms the x-(chordwise) derivatives are differenced with a special split-type method with inherent damping. Special compact upwind- and downwind-biased stencils are used and unconditionally combined in the final timewise corrector step. The Poisson equations for the spectral components

of the wall-normal velocity are solved by a vectorizable stripe pattern LSOR technique, iteratively in x-direction, in conjunction with a FAS multigrid technique with four grid levels. Alternatively, a direct Fourier method can be used to solve the linear systems that is, depending on the number of used cycles in the multigrid method, up to 50% faster. For a detailed description of the DNS method see [1-4].

For the outflow boundary, a self developed and well-tested damping-zone technique is applied, wherein the vorticity disturbance vector is directly forced to zero upstream of the actual outflow boundary. In the case of a skew base flow it is crucial to keep the solenoidality of the vorticity field for the 2-d component – the DC component in the spanwise spectral ansatz – which is identically satisfied in the case of non-skew base flow.

The typical grid sizes used are $2106 \times 2610 \times 257 \times 385 \times 64 \times 256$ points in chordwise (x-), wall-normal (y-), and spanwise (z-) direction, respectively. In the y-direction zones with successively halved Δy can be used; here we used just one zone at the wall with 33 points. A simulation on the vector machine NEC SX-5 with 16 processors, installed at the high-performance computing center Stuttgart, takes about $2.2 \mu\text{s}$ per grid point and full time step on a single processor. The memory requirement is about 150 Bytes per point depending on the online data processing. In the fine resolution case the dominating terms in the time step limit q are the wall-normal viscous term, with $DFL_y = \nu \Delta t / (\Delta y_{\min})^2 \approx 0.25 \approx 0.6 \cdot DFL_{y,\max}$, and the wall-parallel convection terms, with $CFL_x = |u|_{\max} \Delta t / \Delta x$, $CFL_z = |w|_{\max} \Delta t / \Delta z$, both ≈ 0.35 ; ν is the kinematic viscosity, and u and w the total velocity components in chordwise and spanwise direction, respectively. Note that $DFL_y / \Delta t$ is weighted with $k_{\text{mod,max}}^2 = 6.85$ for 6th-order compact FDs in q , and the other terms $CFL_x / \Delta t$, $CFL_z / \Delta t$ with the value of approximately 2~3 for the applied biased 6th-order compact FDs, and π for the Fourier discretization, respectively.

4.2. Results

Carefully verified and validated DNS has established as a self-contained method for transition research. The results shown here are not simulations of an experiment (what in most cases is the best thing to do at first and what we did) but of carefully designed cases summing up the existing and lacking knowledge to elucidate principal physical mechanisms. Rewardingly, some findings could be confirmed by very recent experiments (see [4]). The DNS deliver a complete 3-d unsteady flow field and thus flow structures can be visualized and identified.

4.2.1. Basic physical mechanism

The realistic, superimposed development of CF vortex-mode packets $(0,k)$, $k=1-4$ has been investigated. The discrete waves are presented in the frequency-spanwise wavenumber spectrum, so (h,k) denotes a mode with a frequency h times the fundamental frequency β , and a spanwise wavenumber k times the basic spanwise wavenumber γ . For the individual packet components the initial spanwise phase relation was chosen to model a point-like disturbance like a roughness, and the natural

disturbance background was modeled by a low-amplitude, time-periodic pulse-disturbance.

All modes lie within the unstable region and are amplified just after their excitation leading to a nonlinear development over most of the integration domain. In physical space clockwise-rotating (when looking downstream, left wing), strong vortices are formed which, in the steady case, are oriented along the potential streamline. Upon downstream vortex saturation, the mean flow is deformed resulting in the formation of strong shear layers, which are connected to local inflectional mean profiles $u_s(y)$, $u_s(z)$. (The subscript s denotes the local direction of the potential streamline.) They trigger the explosive growth of secondary instabilities. These instabilities are localized in physical space, i.e. fixed to the primary vortical structure, and appear in the low-momentum upwelling region, where especially the spanwise gradients in the meanflow become extreme. In physical space, the growth of the secondary instability is connected to the appearance of secondary finger-vortices twining around the left, upward moving side of the priming vortex (see fig. 1, at the right vortex). The numerical challenge is in the moving localization and the different scales of the primary and secondary structures, the latter having chordwise wavenumbers up to about 30 times the primary one. Moreover, those structures are not just higher harmonics of the primary mode but are 'linear' secondary modes. The characteristics of the secondary instability strongly depends on the development and nonlinear saturation of the primary crossflow vortex modes with respect to amplification rates, starting point and the dominance of one distinct type of instability. In summary, a regular distribution of vortical strength, i.e. a pattern of equal vortices is less dangerous with respect to triggering secondary instability than a spanwise modulated distribution with the same average value and individual vortices of greater strength. Comparing the crossflow-vortex-mode-packet case with the single-crossflow-vortex-mode case it turns out that the maximum flow deformation, especially the strongest local deceleration of the meanflow is stronger in the packet case. Here, a superposition of mode $(0,2)$ with the odd modes $(0,1)$ and $(0,3)$ is present, resulting in a modulated weak/strong vortex pattern instead of a regular medium/medium pattern in the single-mode cases. In fig. 1 the right vortex is stronger than the left one.

In experiments this packet effect appears not only with randomized roughness but also with a regular artificial roughness row with a spanwise spacing larger than the wavelength of the most amplified mode.

From theoretical work there was some indication that the secondary instability may be of absolute nature, i.e. the disturbances would grow in time while their energy remains at a finite location in space. To corroborate the convective nature of the secondary instability mechanism, the excitation of the periodic background pulses in the vortex-mode-packet case has been switched off after some simulation time. Then the unsteady disturbances are convected downstream and the flow field eventually relaxes fully to a steady state. The temporal evolution of the disturbance amplitudes shows the fast convalescence of the crossflow vortices, indicating the persistence of these flow structures even in early turbulence. The convective nature could have been anticipated already from the possible time-accurate marching to the steady

state in the crossflow-vortex-mode-packet case with saturated steady crossflow vortices in the integration domain. Note that, with an improper DNS method or resolution, it is easy to find spurious absolute instability, or spurious convective instability might only be found with a numerically overstable method that can not reproduce the correct primary and secondary instability growth rates.

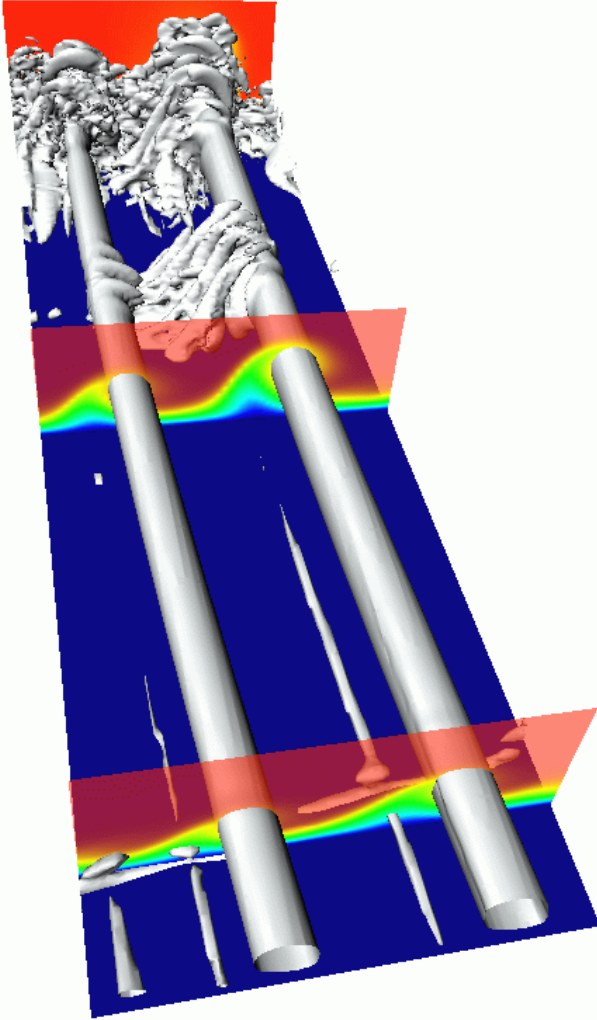


Figure 1. Snapshot of vortical structures (visualized by the λ_2 -criterion method) during crossflow-vortex induced transition in a 3-d boundary layer. The meanflow direction is from bottom to top, the basic crossflow from right to left, black: wall section in edge-streamline system x_s - z_s ; the primary vortices turn clockwise. Periodic background pulses lead to secondary finger vortices first at the left side of the right, stronger primary CF vortex. The cross planes show the time-averaged u_s' -distortion.

4.2.2. Transition delay

For transition delay on swept wings often boundary-layer suction at the wall is used. This method is technically complicated and costly, and has not really proven to work reliably in a satisfactory manner, at least when hole arrays are used. Recently a different method for transition delay came along with the pioneering experiments at the

Arizona State University (ASU) by Bill Saric and co-workers on transition delay on a model wing by artificially forcing vortices with subcritical spanwise spacing (see, e.g., [4]). Mutual suppressions of steady crossflow modes caused by nonlinear interactions led to the idea to induce vortices with a spanwise wavelength smaller than that of the most unstable mode to suppress the latter. For the considered wing profile a delay could indeed be shown. The basic idea of this method, which we name Upstream Flow Deformation (UFD) technique, is to directly influence the crossflow vortex modes most dangerous for triggering secondary instability by a less costly method, in which a spanwise row of artificial roughness is attached near the leading edge, with a roughness spacing smaller than the wavelength of the most amplified mode. By exciting an only weakly unstable crossflow vortex mode with comparably small spanwise wavelength the naturally growing vortices are to be hindered in growth.

Narrow-spaced vortices are less unstable with respect to secondary instability. The crossflow vortex modes with wavenumbers greater than the one of the most amplified mode generate only primary stable higher spanwise harmonics and attenuate further downstream. However, it has been observed that a strong interaction of the crossflow vortex modes is present in nonlinear stages, i.e. the mode attaining an amplitude of about 10% first dominates the scenario by suppressing the other modes. These findings substantiate the method of Saric et al. to enforce high-amplitude crossflow vortices with $2/3$ the spanwise wavelength of the most amplified crossflow vortex mode upon the flow to suppress the most destabilizing modes resulting in a delay of the onset of the secondary instability mechanisms.

From the previous investigations, both theoretical and experimental, a conclusive explanation of the mechanisms acting could not be drawn yet, and it was not clear if the results are valid only for a very specific flow situation. The UFD strategy has been investigated in the boundary-layer flow considered within the scope of this DNS project. It is applied to the crossflow-vortex-mode-packet case, forcing a high-amplitude UFD-mode (0,3) shortly upstream of the original primary disturbances; note that the mode (0,2) is the most unstable. Subsequently, the effect on the individual packet components is investigated, and the modification in the secondary instability properties, and thus the delay of transition has been quantified.

Briefly put, in our computational raster a wavelength of $2/3$ of the most amplified mode turns out to be the optimum for the UFD. In the most relevant simulation an excitation amplitude A_v for the UFD mode (0,3) of 5% $u_{s,e}$ shortly upstream of the excitation point of the vortex-mode packet has been chosen. The UFD mode is amplified first, generating also a large 2-d mean flow distortion, and attains a maximum physical amplitude of 29%; thereafter it decays somewhat. Compared to the reference case without UFD, the development of the other steady modes is clearly suppressed and the UFD mode remains the largest mode throughout the whole integration domain. Next, this steady scenario has been combined with the low amplitude, periodic background pulse disturbance. All unsteady modes are neutrally stable or even damped, and transition is shifted far downstream, see fig. 2.



Figure 2. Snapshots of vortical structures. Left: like fig. 1, but in an extended domain. Right: with upstream flow deformation (UFD), i.e. appropriately enforced narrow-spaced vortices. Transition is shifted far downstream because the background pulses do not grow anymore.

Complementing simulations with varying excitation positions for the background disturbances substantiate these results and exclude that the secondary instability sets in at another downstream position. An explanation for the excellent working of the UFD can be found checking the local (3-d) mean-flow decelerations. Thus it appears that the maximum deceleration, a co-criterion for the secondary instability, significantly decreases with the use of the UFD. This effect is much stronger than could be expected from the different saturation levels of the dominating spectral modes, because in physical space all modes, also the ones nonlinearly generated, superimpose and intensify the 3-d distortion of the mean flow. The deceleration in the UFD cases attains its maximum value far upstream and does not exceed a threshold value.

The goal of transition control is the reduction of skin friction. The UFD strategy applied here can be evaluated theoretically analyzing the local skin friction coefficient c_f' . Typically, c_f' increases drastically due to transition, subject to delay by the UFD strategy. The overall skin friction is significantly less in the UFD cases, although the excitation of the UFD mode causes additional drag first by locally bringing high-momentum fluid to the wall and by the meanflow distortion (0,0).

5. HYPERSONIC CONE BOUNDARY-LAYER: 'ACOUSTIC-MODE' BREAKDOWN

Laminar-turbulent transition in super- and hypersonic boundary layers does not only have strong influence on shear stresses and heat flux, but also on other flow phenomena like shock/boundary-layer interaction and flow separation, and can therefore influence the global flow field and the aerodynamic drag substantially. For air-breathing propulsion systems of the lower stage of space vehicles a thin laminar boundary layer on the forebody, designed to compress the air before the flow enters the engine intake, is clearly favorable. For transition studies generic bodies like flat plates or cones are used that are also employed as basic forebody geometries. Investigations using local Linear Stability Theory (LST) could deliver an overview of the amplification of small-amplitude disturbance waves at different wall-temperature conditions, and revealed for Mach numbers higher than 2.2 an amplified, so-called acoustic disturbance mode (or 2nd mode) in addition to the vorticity mode (1st mode) known from incompressible flow. This acoustic mode is most amplified if it is 2-d, grows stronger than the vorticity mode for a Mach number higher than 4, and is destabilized by wall cooling. It is connected to the appearance of a region near the wall where the disturbance mode moves faster than sound waves can travel, see fig. 3. Note that the phase speed of the disturbance wave is indeed approximately constant in wall-normal direction, and that wall-cooling enlarges the 'supersonic' region because the sound speed (a) near the wall is decreased compared to the adiabatic case.

In investigations using the Parabolized Stability Equations (PSE) that allow for non-parallelism of the base flow and weakly nonlinear stages, a sensitivity of the results with respect to the base-flow accuracy has been found. Transition typically proceeds much slower than in subsonic flow, and the (weakly) nonlinear region can be very long. Thus base flow errors can have a strong influence on the downstream development, and accurate full Navier-Stokes solutions are favorable.

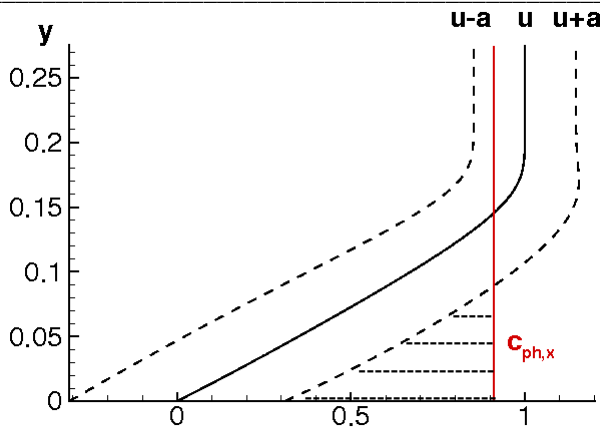


Figure 3. Boundary-layer velocity profiles showing the local region with ‘supersonic’ disturbance speed (horizontal, dashed lines), causing acoustic-mode instability.

In the rare wind-tunnel experiments transition is usually caused by uncontrolled background disturbances in the oncoming flow. From a historical point of view, transition has been observed at first to take place earlier on the flat plate than on the cone in ‘cold’ experiments – with a stagnation temperature equal to about the ambient temperature and under uncontrolled conditions –, contrary to LST predictions. Nowadays, investigations in ‘quiet’ tunnels and in-flight experiments indicate that this was caused by the wind-tunnel noise in connection with strong disturbance receptivity on the flat-plate’s leading edge, representing a line compared to the apex of the cone. For the American Project Hyper-X (X-43) indeed a wedge-like forebody has been chosen rather than a conical shape. For an in-depth interpretation and careful comparisons with stability theories and DNS, controlled experiments in quiet tunnels with controlled disturbance input are essential. A first controlled experiment on a cone in hypersonic flow has been performed by Maslov et al. (2000) at ITAM, Novosibirsk (see [7]), and is presently simulated at IAG.

Down to the present day all investigations of other research groups on nonlinear breakdown phenomena in super- and hypersonic flow are concerned with cold boundary layers at wind-tunnel conditions. In the work discussed here transition is examined at flight conditions in the atmosphere, with realistic wall-cooling by radiation.

5.1. Numerical method

The results are gained with a carefully tested 6th-order compact FD / azimuthal Fourier-spectral scheme for spatial DNS in conservative formulation using the

variables (ρ , ρu , ρv , ρw , e), ρ - density, e - internal energy, in the domain shown in fig. 4 with periodic sidewise boundaries. It is body-fitted and does not contain the shock sheet from the apex. First, the steady non-self-similar base flow is calculated using the full equations including body divergence and transverse curvature. It is well-defined by the inflow profiles obtained from self-similar flat-plate solutions adapted to the cone, and an upper boundary condition based on spatial (x - y -plane) conical characteristics. The fluid is a thermally perfect gas, and for the wall temperature T_w we use a radiation-adiabatic condition where the heat flux into the wall, connected to the slope of the $T(y)$ -profile, is instantaneously balanced by the radiated flux that is proportional to T_w^4 . Defined disturbances are introduced in a strip at the wall by localized blowing and suction, prescribing $(\rho v)'$, ‘marking the disturbance, and their 3-d, symmetric, unsteady development up to late stages of transition is simulated in disturbance formulation. The latter allows different boundary conditions for base and disturbance flow. At the upper boundary a theoretically non-reflecting y - t -plane characteristic condition is applied. For time integration an RK4-O4 method is used.

In the pseudospectral method for the nonlinear terms the x -derivatives are differenced with a special split-type method with inherent damping. Special compact upwind- and downwind-biased stencils are used and unconditionally combined in the final timewise corrector step. The de-aliasing/damping properties for high wavenumber components have to be stronger than in the incompressible case because the nonlinearity is superquadratic (see [1]).

Near the outflow boundary a damping-zone technique is applied, wherein all disturbance variables are directly ramped to zero. This is equivalent to the ‘sponge-layer technique’ with implicit treatment of an artificial damping term that, in our method, can be infinitely large.

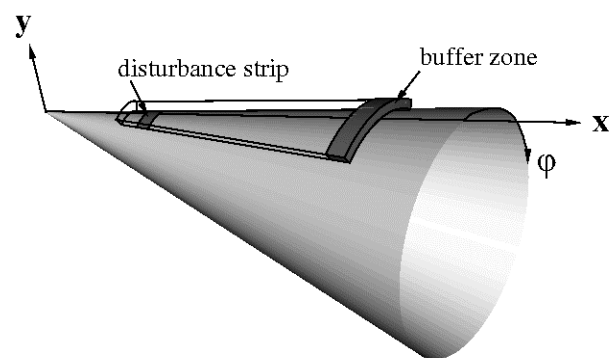


Figure 4. Cone coordinate system and body-fitted integration domain.

The typical grid sizes used are $2400\text{-}2600 \times 169 \times 32(64)$, points in x -, y -, and circumferential direction, respectively. In the y -direction zones with successively halved Δy can be used; typically two zones near the wall are applied. Note that the largest gradients in the unsteady flow do not always appear at the wall. A simulation on the NEC SX-5 takes about $3.8\mu\text{s}$ per computed grid point and full time step on a single processor. The memory requirement is

about 300 Bytes per point depending on the online data processing. For the fine resolution the dominating terms in the time step limit q are the wall-normal viscous term, with $DFL_y = \mu/\rho \cdot \Delta t / (\Delta y_{min})^2 \approx 0.2 \approx 0.5 \cdot DFL_{y,max}$, and the wall-normal convective term $CFL_y = (|v|+a)\Delta t / \Delta y \approx 0.2 \approx 0.18 \cdot CFL_{y,max}$; μ is the viscosity, and a the speed of sound. Compared to the incompressible case here often the wall-normal convective term prevails due to the inclusion of the sound propagation in the equations directly subject to time integration. Note that $DFL_y/\Delta t$ is weighted with $k_{mod,max}^2 = 6.85$ for 6th-order compact FDs in q , and $CFL_y/\Delta t$ with the value of approximately 2~3 for the applied biased 6th-order compact FDs (cf. [1]).

5.2. Results

For the simulations we choose flight conditions, i.e. 'hot' flow with $T_\infty = 220K$ at $M_{edge} = 6.8$, and radiation-adiabatic cooled wall with $T_w \approx 0.5 \cdot T_{rec} \approx 975K$. A specialty on the cone is that the (basic) azimuthal wavenumber is defined by $\gamma = n/r$ with n constant and $\gamma_0 = n/R_0$; n represents the spanwise (integration-domain) wavelength as an integer fraction of the circumference: $n=2$ means that the wavelength covers half the circumference. r denotes the radial distance of a point from the cone axis, thus $\gamma = \gamma_0 R_0/r$. Going downstream, all considered azimuthal wave numbers and the respective wave propagation angles reduce with the increasing radius, i.e. all modes tend to become 2-d.

Oblique-type transition induced by a symmetrical pair of vorticity-type waves ($1, \pm 1$) is found to be a robust mechanism, active on both the flat-plate and the cone. (This holds also for wind-tunnel and flight conditions. The higher temperature at hot flow and the wall-cooling stabilize however this 1st mode. In the past this led to the conclusion that transition takes place more upstream in cold wind-tunnel experiments than at flight conditions which is only true for this type of scenario.)

In the fundamental-type transition scenario an acoustic 2-d primary disturbance ($1,0$) and a secondary 3-d mode ($1, \pm 1$) with the same frequency, but small amplitude, are excited. The frequency parameter is $F = 2\pi f^* / (u_\infty^* \cdot Re_L) = 10 \times 10^{-5}$ for the cone; the asterisk marks dimensional values. The 2-d primary wave ($1,0$) grows due to the primary instability. At a threshold amplitude, the phase speed of the secondary 3-d mode starts to synchronize with the primary wave; after adaptation resonant growth of ($1, \pm 1$) and the nonlinearly generated ($0,1$) takes place. Since the 2-d and 3-d 2nd-mode waves tend to be the same going downstream on the cone due to the natural reduction of the azimuthal wave number, their phase speeds do similarly. This renders the necessary threshold amplitude on the cone to be only half that on the flat plate: it is $u'/u_\infty \approx 4\%$.

For the likeliness of the different transition scenarios at flight conditions with wall-cooling we find the following: The unstable region begins quite early for 3-d vorticity modes, and three times earlier on the flat plate than on the cone. Since the relevant 2-d-mode integral amplification, decisive for fundamental breakdown, is reached only late on the flat plate, oblique breakdown is expected to be the most relevant mechanism there. On the cone however, sufficiently large 2-d-mode integral

amplification is reached earlier and the behavior of the secondary 3-d waves accelerates the fundamental mechanism as described above. Here, fundamental transition caused by 2-d acoustic modes significantly destabilized by the wall-cooling is likely to be the dominant mechanism.

The possibility of the appearance of fundamental breakdown on the cone has an important consequence in practice. It is a mechanism caused by acoustic disturbances which have their maximum located near the wall. Therefore the heating of the wall in the transitional regime is much larger than in the oblique-type scenario. This is verified by the examination of the wall temperatures computed using the radiation-adiabatic wall-temperature condition for the instantaneous total flow. The time-averaged wall-temperature increase for the fundamental case on the cone is shown in fig. 5. The heating in the computed area reaches 250K, which is more than 25% of the wall temperature, about 975K, of the laminar base flow.

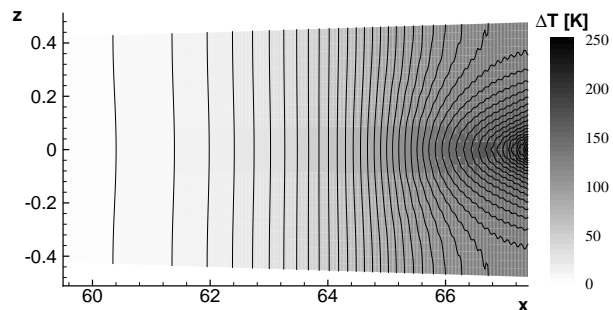


Figure 5. Time-averaged wall-temperature increase during fundamental-type transition at $M_e = 6.8$ on the cone with radiation-adiabatic wall cooling.

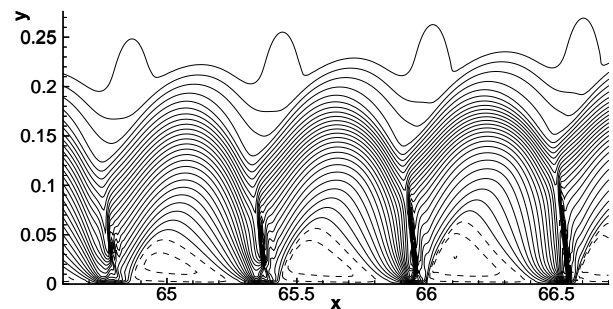


Figure 6. Isocontours of instantaneous velocity component u/u_∞ in longitudinal flow cut showing local separation regions and shocklets caused by a large-amplitude acoustic mode; for fundamental-type transition at $M_e = 6.8$ on the cone with wall cooling. The increment is 0.04 and negative values are dashed.

High-amplitude acoustic modes cause complex physical phenomena. These disturbances have the special characteristic that they travel by more than the speed of sound faster than the base flow in a relative supersonic region near the wall. However, this only holds if the amplitudes are small. As the amplitudes increase, we observe the formation of shocklets. They can be clearly

seen in fig. 6 where isolines of the instantaneous u-component are plotted. Dashed lines correspond to negative values, so strong local flow separation areas are also visible. They are caused by the presence of the strong 2-d wave with its near-wall maximum, at a still relatively low mean-flow distortion near the wall. The simulation of these phenomena needs an enormous computational effort, and the simulations can not yet be easily extended into later stages. (Are there any Λ -vortices like in subsonic flow?) We incessantly work on it. More details of our DNS of super-/hypersonic boundary-layer transition can be found in [5-7].

6. ACKNOWLEDGEMENTS

The DNS were performed by Peter Wassermann for the crossflow case and by Axel Fezer for the hypersonic case; I greatly appreciate their contributions. The financial support of the Deutsche Forschungsgemeinschaft under contracts KI 890/2 and SFB259-TP-C4-KI/Wa as well as the support by the high-performance computing center Stuttgart, HLRS, within the project LAMTUR are gratefully acknowledged.

I apologize for the compact literature list. Important contributions of other authors are cited in the papers given.

7. LITERATURE

- [1] Kloker, M. (1996): Katalog 1 - Numerische Löser (Zeitintegrationsverfahren) für die gewöhnliche Differentialgleichung $y'=\alpha y$, α komplex. *Lösungseigenschaften von Finite-Differenzen-Verfahren: Diagrammkatalogreihe. Lecture catalogue*, IAG, 35 pages.
- [2] Kloker, M. (1998): A robust high-resolution split-type compact FD-scheme for spatial direct numerical simulation of boundary-layer transition. *Applied Scientific Research* 59, 353-377.
- [3] Bonfigli, G., Kloker, M. (1999): Spatial Navier-Stokes simulations of crossflow-induced transition in a 3-d boundary layer. In *New Results in Numerical and Experimental Fluid Dynamics II* (ed. Nitsche, W.; Heinemann, H.-J.; Hilbig, R.), Proc. 11th AG STAB/DGLR Symposium, 1998, Berlin. Notes on Numerical Fluid Mechanics 72, 61-68, Vieweg.
- [4] Wassermann, P.; Kloker, M. (2002): a) Mechanisms and passive control of crossflow-vortex-induced transition in a three-dimensional boundary layer. *J. Fluid Mech.* 456, 49-84. b) Transition mechanisms induced by traveling crossflow vortices in a three-dimensional boundary layer. Accepted for publication in *J. Fluid Mech.*
- [5] Fezer, A.; Kloker, M. (1999): Transition processes in Mach 6.8 boundary layers at varying temperature conditions investigated by spatial DNS. In *New Results in Numerical and Experimental Fluid Dynamics II* (ed. Nitsche, W.; Heinemann, H.-J.; Hilbig, R.), Proc. 11th AG STAB/DGLR Symposium, 1998, Berlin. Notes on Numerical Fluid Mechanics 72, 138-145, Vieweg.
- [6] Fezer, A.; Kloker, M. (2000): Spatial direct numerical simulation of transition phenomena in supersonic flat-plate boundary layers. In *Laminar-Turbulent Transition*. Proc. IUTAM Symp., Sedona, Az, USA 1999 (ed. Fasel, H.; Saric, W.), Springer.
- [7] Fezer, A.; Kloker, M. (2002): DNS of transition mechanisms at Mach 6.8 – flat plate vs. sharp cone. *Proc. West East High Speed Flow Fields 2002* (ed. Zeitoun, D.E.; Periaux, J.; Desideri, A.; Marini, M.), Marseille, 2002. © Cimne, Barcelona, Spain.